

PREPARED FOR SUBMISSION TO JINST

8TH SYMPOSIUM ON NEGATIVE ION BEAMS AND SOURCES

OCTOBER 3-7, 2022

PADOVA (ITALY)

Measure of negative ion density in a large negative ion source using Langmuir probes

C. Poggi,^a M. Spolaore,^a M. Barbisan,^a M. Brombin,^a R. Cavazzana,^a N. Marconato,^{a,b} R. Pasqualotto,^a A. Pimazzoni,^a E. Sartori,^{a,b} and G. Serianni^a

^a*Consorzio RFX (CNR, ENEA, INFN, Università di Padova, Acciaierie Venete SpA),
Corso Sati Uniti 4, 35127, Padova, Italy*

^b*Università degli Studi di Padova,
Via VIII Febbraio 2, 35122, Padova, Italy*

E-mail: carlo.poggi@igi.cnr.it

ABSTRACT: Neutral Beam Injectors (NBIs) based on negative ions are the workhorses of future fusion reactors, such as ITER, which they are expected to provide with up to 33 MW of power to heat the fusion plasma. The negative hydrogen ions are extracted from a RF plasma, in which a magnetic filter field cools down the electrons reaching the so-called expansion region and allows the formation of negative ions near the apertures in the plasma grid. To further improve the production of negative ions, cesium is usually evaporated inside the source and deposited onto the plasma walls, reducing the work function of the surfaces. This dramatically increases the density of negative hydrogen ions near the surfaces, causing the transition to an electronegative plasma in the vicinity of the plasma grid. This condition can be observed with Langmuir probes.

In this paper we use the measurements provided by the Langmuir probe system embedded in the plasma grid of SPIDER, the prototype ion source of ITER NBIs, to determine the density of negative ions. A fitting method based on the determination of the collection area of the different plasma species is proposed and adapted to SPIDER experimental condition, taking into account the shape of the probes and the local topology of the magnetic field. The method is then applied to the experimental data, determining the densities of the positive and negative ions and of the electrons during a plasma pulse. Finally, a vertical array of four probes in the plasma grid is used to assess the vertical profile of plasma parameters.

KEYWORDS: Ion sources, Plasma diagnostics - probes

¹Corresponding author.

Contents

1	Introduction	1
2	Model of the Langmuir probe characteristic	2
2.1	Evaluation of the collection areas	4
2.2	Fitting of the data and error estimation	6
3	Application to the experimental data	7
4	Conclusion	9

1 Introduction

Neutral beam injectors for future fusion reactors like ITER require charged beams up to 1 MeV of energy to be used as precursor [1]. For this reason they rely on negative ion sources to produce the required beam current density, that for ITER is set at 330 A/m^2 for neutral hydrogen beams. The SPIDER experiment (Source for the Production of Ions of Deuterium Extracted from a Radio-frequency plasma), hosted at Consorzio RFX in Padova, is the full-scale prototype of ITER neutral beam injectors [2, 3]. It consists of a plasma chamber made of 8 cylindrical drivers inside which an inductively coupled plasma discharge is generated using four 1 MHz RF generators capable to deliver up to 800 kW of total power. The plasma then protrudes inside the so-called expansion chamber towards the plasma grid, from which negative ions are extracted through 1280 apertures, organized in 4 vertical segments of 4 beamlet groups of 80 beamlets each. A mostly horizontal magnetic filter field is generated inside the expansion region by a current flowing vertically in the plasma grid. This magnetic field cools down the electrons generated inside the drivers, allowing the formation and survival of the negative hydrogen ions near the plasma grid apertures. A further electrode, called bias plate, is placed at 1 cm from the plasma grid and frames all the beamlet groups. Both the plasma grid and the bias plate electrode can be biased with respect to the other source walls. The control is usually performed over the total current flowing between the electrode and a protection resistor of 0.6Ω [4]. To increase the surface production of negative ions, cesium is evaporated inside the source from three cesium ovens, placed between the plasma grid segments, and it is deposited over the plasma facing surfaces [3, 5, 6].

SPIDER is equipped with several Langmuir probes embedded in the plasma grid and bias plate electrodes [7, 8]. The probes were operated during SPIDER operation, providing information about plasma parameters and source uniformity [9]. Some of them were polarized with voltage ramps, in order to measure the current-voltage characteristics. Cesium injection leads to the occurrence of a nearly ion-ion plasma condition near the plasma grid, characterized by large value of the electronegativity parameter at the sheath edge $\alpha = n_-/n_e$, given by the ratio of the negative ion and electron densities. This transition to an ion-ion plasma is characterized by a decrease of the

electron saturation branch of the measured Langmuir probe characteristics, so that standard methods to analyze the I-V curves like 4-parameter fitting of the positive ion branch or second derivative analysis of the electron branch cannot be used. In this paper we apply the method described in the work by Bredin et al [10] to fit the entire characteristic, taking into account the different magnetizations of electrons and ions, affecting the collection area of the different species. The model is described in section 2, while its application to SPIDER experimental data is reported in section 3.

2 Model of the Langmuir probe characteristic

The Langmuir probe electrodes embedded in SPIDER plasma grid and bias plate consist of cylinders with a radius $R_{pr} = 3.5$ mm protruding by an height $h = 1$ mm inside the plasma, for a surface exposed to the plasma $S_{geom} = 60$ mm². Each probe is embedded and isolated within the corresponding plasma facing grid with a gap of 0.25 mm surrounding the electrode.

The Langmuir probe I-V characteristic is modelled considering the contributions of the different plasma species: electrons, positive ions and negative ions. Given the densities of positive and negative ions and of the electrons at the sheath edge (n_+^s , n_-^s and n_e^s respectively), their masses (m_+ , m_- , m_e) and their temperatures (T_+ , T_- , T_e), imposing quasi-neutrality ($n_+^s \approx n_-^s + n_e^s$), below the sheath potential V_s the collected electron, positive and negative ion currents behave as:

$$I_e(V) = \frac{1}{4} e S_{eff}^e v_e \frac{n_+^s}{1 + \alpha_s} \exp\left(e \frac{V - V_s}{T_e}\right) \quad \text{with } v_e = \sqrt{\frac{8T_e}{\pi m_e}} \quad (2.1a)$$

$$I_+(V) = e S_{eff}^+ (V) u_B^+ n_+^s \quad \text{with } u_B^+ = \sqrt{\frac{T_e}{m_+}} \sqrt{\frac{1 + \alpha_s}{1 + \gamma \alpha_s}} \quad (2.1b)$$

$$I_-(V) = e S_{eff}^- (V) n_+^s u_B^- \frac{\alpha_s}{1 + \alpha_s} \exp\left(e \frac{V - V_s}{T_-}\right) \quad \text{with } u_B^- = \sqrt{\frac{T_+}{m_-}} \quad (2.1c)$$

where $\alpha_s = n_-^s/n_e^s$ is the electronegativity parameter at the sheath edge, S_{eff}^e , S_{eff}^+ and S_{eff}^- are the electron, positive and negative ion effective collection areas of the probe, v_e is the mean velocity of a Maxwellian electron population, u_B^+ is the modified Bohm velocity considering negative ions and considering also the electron to ion temperature ratio $\gamma = T_e/T_-$, and u_B^- is the negative ion Bohm velocity [11]. For $V > V_s$ the currents are instead given by:

$$I_e(V) = \frac{1}{4} e S_{eff}^e v_e \frac{n_+^s}{1 + \alpha_s} \left(2 \sqrt{e \frac{V - V_s}{\pi T_e}} + \exp\left(e \frac{V - V_s}{T_e}\right) \text{erfc}\left(\sqrt{e \frac{V - V_s}{T_e}}\right) \right) \quad (2.2a)$$

$$I_+(V) = e S_{eff}^+ (V) u_B^+ n_+^s \exp\left(e \frac{V_s - V}{T_+}\right) \quad (2.2b)$$

$$I_-(V) = e S_{eff}^- (V) n_+^s u_B^- \frac{\alpha_s}{1 + \alpha_s} \quad (2.2c)$$

with the electron current being described by the standard OML theory [12].

An example showing the various contributions of equations 2.1 and 2.2 to the total current is presented in figure 2a (parameters are $n_+^s = 1 \times 10^{17}$ m⁻³, $T_e = 2$ eV, $T_+ = 0.8$ eV, $T_- = 1.5$ eV, $T_- = 1.5$ eV, $m_+ = 1.8$ amu). Fitting a voltage-current characteristic with this model can in principle

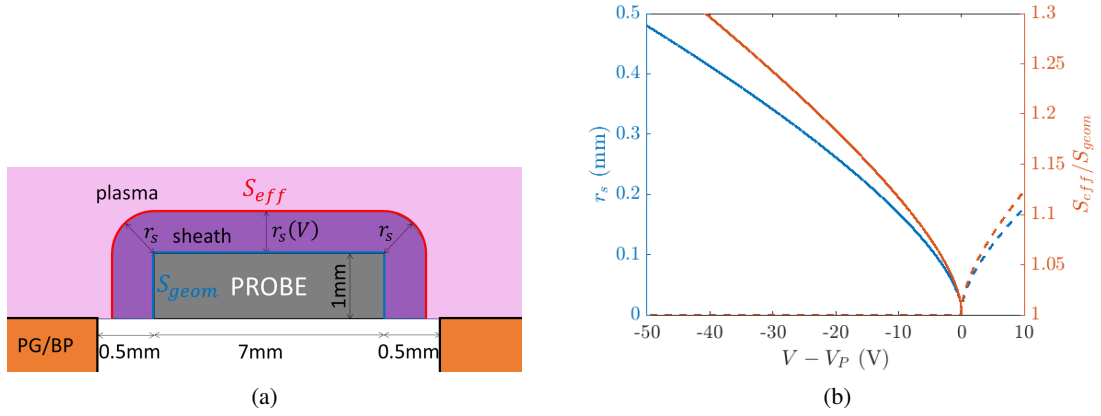


Figure 1: (a) Schematic section of a SPIDER Langmuir probe, showing its dimensions and the difference between the geometrical and the effective ion collection areas. (b) Dependence of the sheath size and of the S_{eff}^{\pm}/S_{geom} ratio on the probe polarization voltage.

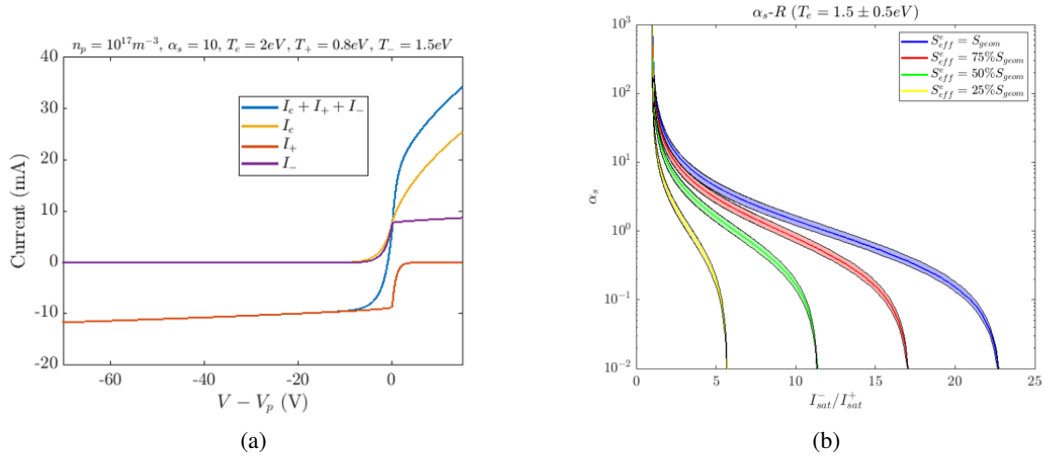


Figure 2: (a) Plot of the model described by equations 2.1 and 2.2, showing the contributions coming from the different plasma species. (b) Dependence of the electronegativity on the ratio between the negative and positive saturation currents, for various values of S_{eff}^e .

provide sheath density and temperature for all the various species that compose the plasma. However, it is necessary to carefully estimate the effective collection areas of all the species, as it is evident from figure 2b: here the electronegativity is plotted against the ratio between the negative and positive saturation currents (the temperatures are $T_e = 2 \pm 0.5$ eV, $T_+ = 0.8$ eV, $T_- = 1.5$ eV, $T_- = 1.5$ eV) for different values of S_{eff}^e/S_{geom} , showing a great variation of the trends for an electronegativity ranging from 0 to 10. Next section is dedicated to describing the calculation of the effective areas for all the species.

2.1 Evaluation of the collection areas

For the positive ions, the collection area is given by the geometrical surface for probe polarization at the plasma potential or above, while for $V < V_s$ it increases with the positive sheath size r_s^+ , as represented in figure 1a. The increase can be calculated as

$$S_{eff}^+ = S_{geom} + 2\pi r_s(V)h + \pi^2 R_{pr} r_s(V) + 2\pi r_s^2(V) \quad (2.3)$$

that accounts for the increase in the lateral area of the cylinder ($2\pi r_s(V)h$) and for the rounded area of curvature radius r_s (the term $\pi^2 R_{pr} r_s(V) + 2\pi r_s^2(V)$ corresponds to the area of a quarter of torus).

The r_s^+ is calculated solving a 1-dimensional Child-Langmuir model [10]:

$$\begin{cases} \frac{dV}{dx} = -E \\ \frac{du}{dx} = \frac{eE}{m_+ u(x)} \\ \frac{dE}{dx} = \frac{n_+^s e u_B^+}{\epsilon_0 u(x)} \end{cases} \quad (2.4)$$

with starting conditions $u(0) = u_B^+$ and $E(0) = 0$. The sheath size is then the x coordinate corresponding to $V - V_s$.

A similar approach is used to calculate the sheath size for the negative ions, solving the system in (2.4) for $V > V_s$ with the negative ion Bohm velocity u_B^- and the negative ion sheath density n_-^s , and setting $r_s^- = 0$ for $V < V_s$. The plots of the sheath sizes r_s^\pm and the corresponding S_{eff}^\pm / S_{geom} are shown in figure 1b, covering the typical range of the probe polarization voltage for a plasma with $n_+^s = 1 \times 10^{17} \text{ m}^{-3}$, $\alpha_s = 5$, $T_e = 2 \text{ eV}$, $T_+ = 0.8 \text{ eV}$, $T_- = 1.5 \text{ eV}$ and an effective positive ion mass $m_+ = 1.8 \text{ a.m.u.}$. As it can be noticed, the sheath size can increase the collection by more than 30 % at large polarization values, and needs to be taken into account.

A different approach is used to estimate the electron effective collection area S_{eff}^e . The magnetic field in correspondence of the probes position is given by the superposition of the filter field generated by the plasma grid current, and the co-extracted electron suppression magnets embedded in the extraction grid, and it presents a significant variation over the probe size, as it is shown in Figure (a). The total magnetic field ranges between 2 and 8 mT over the probe surface, while the electron temperature is around $T_e = 2 \text{ eV}$. In this condition, the electron cyclotron frequency f_{ce} is between 56 and 230 MHz, and the average gyroradius R_{ce} is between 2.7 and 0.7 mm for the particles with speed $\sqrt{kT_e/m_e}$. This value is smaller than the 3.5 mm radius of the probe, but larger than its 1 mm height, and it is therefore not straightforward to determine if the electrons are magnetized or not with respect to the probe size: which is the most relevant size to consider depends on the direction of the magnetic field lines intercepting the probe surface, and this depends on the probe location and the intensity of the filter field current.

The intensity of the magnetic field was calculated numerically using COMSOL and integrated over the cylindrical surface of the probe in order to determine the average magnetic field on the probe surface

$$\vec{B}_\perp = \int_{S_{geom}} \frac{\vec{B}}{S_{geom}} dS \quad (2.5)$$

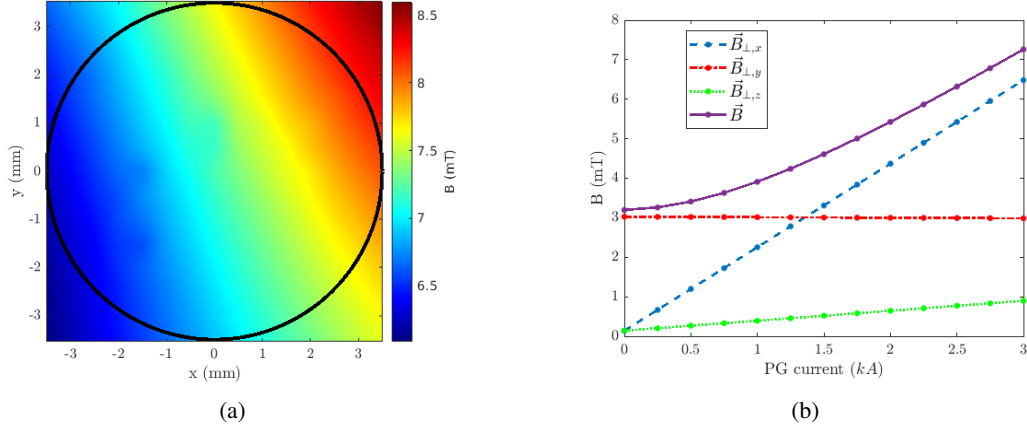


Figure 3: (a) Magnitude of the magnetic field on the surface of a plasma grid probe, for $I_{PG} = 3$ kA. (b) Cartesian components and magnitude of the average magnetic field perpendicular to the probe, \vec{B}_\perp , for different values of plasma grid current.

and the surface perpendicular to the magnetic field

$$S_\perp = \int_{S_{geom}} \frac{|\vec{B} \cdot \hat{n}|}{B} dS \quad (2.6)$$

with \hat{n} the normal to the surface. From this, an effective probe dimension can be determined as $R_{eff} = \sqrt{S_\perp/\pi}$, to be compared with the electron gyroradius calculated for the perpendicular magnetic field B_\perp . Using numerical simulations of the magnetic field [13] allows to take into account the correct topology of the magnetic field in SPIDER expansion region and in particular at probe location: due to the superposition of the contributions coming from the permanent magnets embedded in the extraction grid and the current flowing in the plasma grid, the magnetic field intensity and direction can significantly vary even over the probe size, as it is shown in Figure 3a, where the intensity of the magnetic field over the top surface of one of the plasma grid probe in SPIDER bottom segment is presented. The cartesian components of the \vec{B}_\perp field for various I_{PG} are instead plotted in figure 3b. While the PG current mostly modifies the horizontal x component of the field, the others have a comparable magnitude, with the total field spanning from 3 to 7 mT. The other plasma grid probes present similar values of magnetic field with small differences due to the exact probe location.

According to Usoltceva et al [14] the factor $\beta = R_{eff}/R_{ce}$ controls the passing of S_{eff}^e from S_{geom} to S_\perp as effective surface for the electron collection at plasma potential for a thin cylindrical probe immersed in a magnetic field parallel to the cylinder axis, following the equation

$$S_{eff}^e = S_{geom} \exp(-\beta^2/2) + S_\perp (1 - \exp(-\beta^2/2)). \quad (2.7)$$

The same approach is applied in this paper although in SPIDER the probe orientation with respect to the magnetic field is different, as it can be deduced from figure 3b. A typical trend of $\exp(-\beta^2/2)$ as a function of I_{PG} for a probe embedded in the plasma grid (PG42) and another embedded in the bias plate (BP42, at approximately 10 mm from PG42 along z direction), with

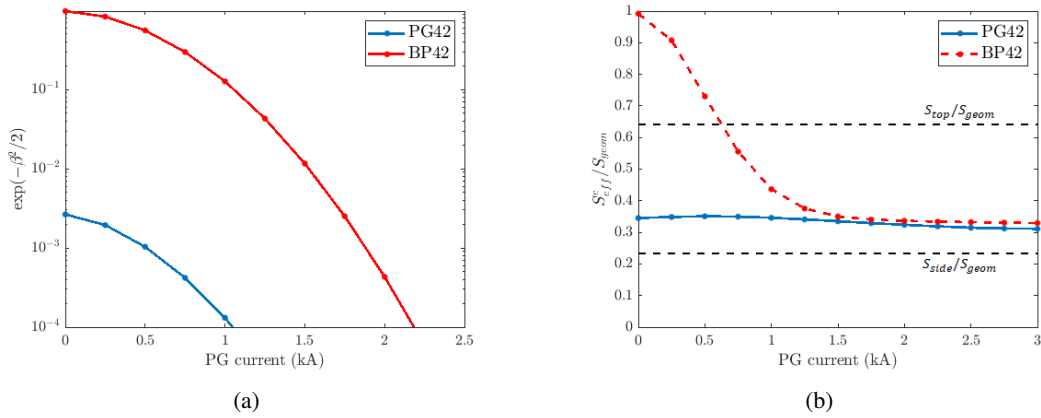


Figure 4: Dependence on I_{PG} of (a) $\exp(-\beta^2/2)$ assuming $T_e = 2$ eV and (b) of the ratio S_{\perp}/S_{geom} for a plasma grid and a bias plate probe located in the bottom segment of SPIDER.

an electron temperature of 2 eV is shown in figure 4a, while figure 4b presents the corresponding S_{eff}^e/S_{geom} ratio. As it can be noticed, while for the plasma grid probe it is always below 1%, for the bias plate probe it can go up to 1 for low plasma grid currents, and goes below 10% for $I_{PG} > 1$ kA. The black dashed lines show the fraction of the total surface that corresponds to the top surface of the probe (top line) and to the projection of the lateral surface (bottom line). As it can be noticed, for both probes the effective area calculated with equation 2.7 is different from those reference values.

With this approach, it was possible to determine the effective collecting areas of the different plasma species, starting from the measurement of the plasma grid current and assuming the effective mass of the positive ions to be known.

2.2 Fitting of the data and error estimation

The model described in the previous section was applied to the Langmuir probe data acquired during SPIDER campaigns. A non-linear least-square algorithm was used to estimate the fitting parameters n_+^s , α_s , T_e and V_s for a measured voltage-current characteristic. The positive and negative ion temperature were fixed at 0.8 and 1.5 eV respectively, as they cannot be easily derived from the Langmuir probe data (although they are present in the model described in previous section). The effective positive ion mass is set at $m_+ = 1.8$ a.m.u. as usually done for similar ion sources [15]. However, this value was never directly measured in SPIDER. As it can in principle vary between 1 and 3 a.m.u., depending on the relative fraction of H^+ , H_2^+ and H_3^+ , a 20% RMS error bar was assumed for it. Concerning the effective electron collection area described above, this depends on the accuracy of the magnetic field simulations, which was taken into account by assuming a 10% RMS error on the value of S_{\perp} . To assess the effect of these error sources to the parameter estimation, fits for randomly generated values of m_+ and S_{\perp} were performed on selected voltage-current characteristics, and the RMS of the corresponding resulting parameters distributions were calculated. This yielded 0.1 eV of RMS error on T_e , a 10% relative error on n_+^s , n_e^s and n_-^s , 20% on α_s and 0.2 V of RMS error on V_s . These errors were then added in quadrature to the uncertainties

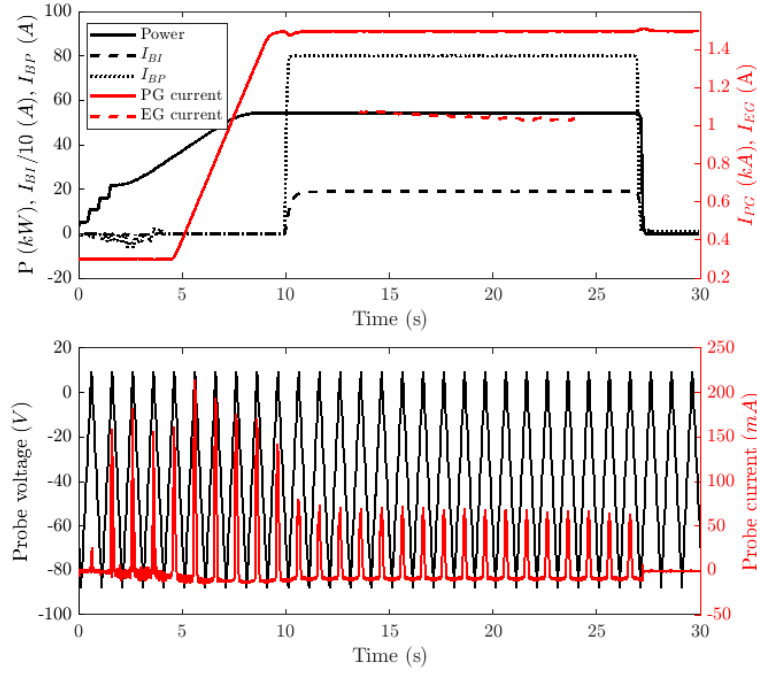


Figure 5: Machine parameters (top) and Langmuir probe PG12 signals (bottom) during a plasma blip with $P_{RF} = 50 \text{ kW/driver}$, $I_{BI} = 190 \text{ A}$, $I_{BP} = 80 \text{ A}$, $I_{PG} = 1.5 \text{ kA}$ at 0.3 Pa of source filling pressure. Extraction voltage is $V_{EG} = 3 \text{ kV}$.

obtained from the covariance matrix given by the fitting routine.

3 Application to the experimental data

The model was applied to the data collected during SPIDER experimental campaigns, allowing to follow the evolution of plasma parameters during the plasma pulses. Standard plasma blips of 27 s were repeated every 4 minutes during most of the day during the campaigns with cesium evaporation. The plot of machine parameters during a plasma blip is shown in figure 5. The top graph shows the trends of machine parameters: power per driver, plasma grid bias (I_{BI}) and bias plate (I_{BP}) current, plasma grid filter current (I_{PG}) and extraction grid current (I_{EG}), while the bottom graph presents the voltage (in black) and current (in red) signals measured by the Langmuir probe embedded in the center of the plasma grid in correspondence of the top segment.

As it can be noticed, from 10 to 28 seconds of each plasma blip the machine parameters were kept constant, and from 14 to 24 seconds beam extraction was performed. This time interval was chosen for the analysis of the probe data. A plot of the fitted plasma parameters for this plasma blip during beam extraction is reported in figure 6, with an example of fitted data reported in figure 6a. Figure 6b indicates that positive and negative ion densities remain constant, while the electron density slightly decreases by 9 %. This is in agreement with the trend of the extraction grid current reported in figure 5, which also decreases by 9 %. The estimated electronegativity α is around 2.4, also slightly increasing due to the electron density reduction, while the sheath potential remains at

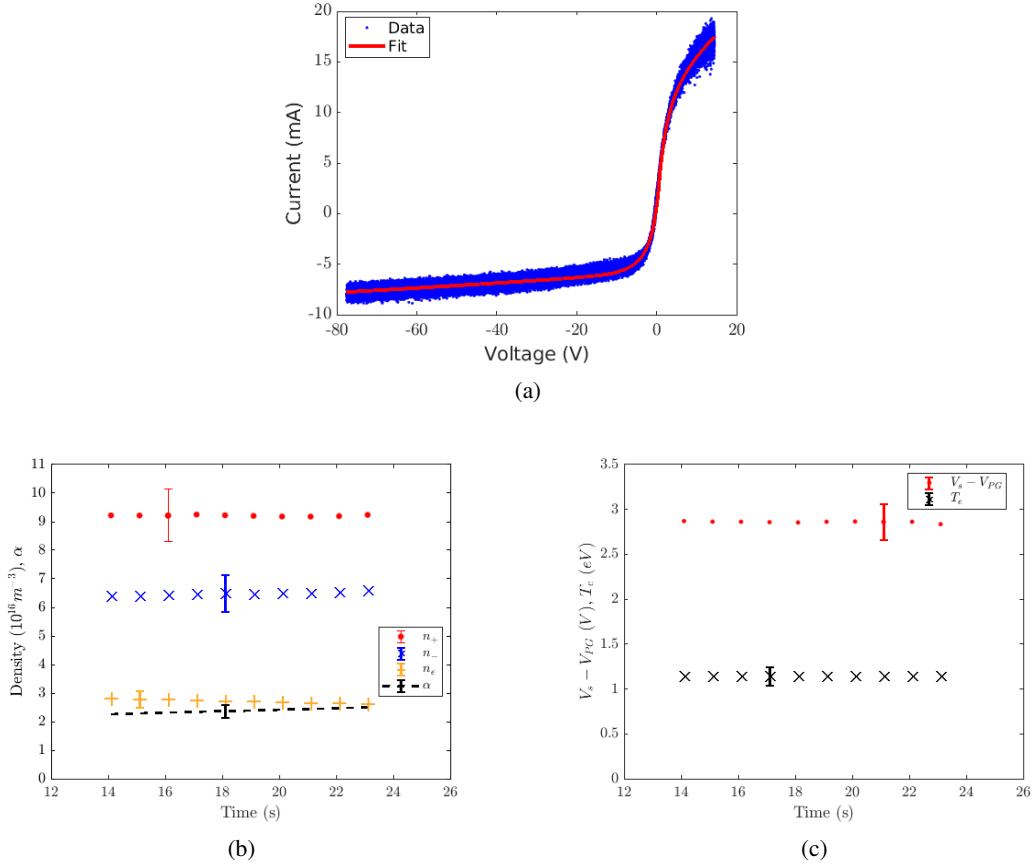


Figure 6: Trend of plasma parameters during the plasma blip of figure 5. (a) Example of the fitted current-voltage characteristic. (b) Densities. (c) Electron temperature, electronegativity and plasma sheath potential referred to the plasma grid.

2.8 V with respect to the plasma grid potential (figure 6c). The measured electron temperature is 1.2 eV, and does not vary during the blip (figure 6c).

A vertical arrangement of four probes in the middle of the plasma grid, one per segment, was used to characterize the vertical plasma uniformity, confirming what was observed also with other diagnostics [17]. Figure 7 compares the fit results obtained from these probes for two plasma blips with $P_{RF} = 50 \text{ kW/driver}$, $I_{BI} = 190 \text{ A}$, $I_{BP} = 80 \text{ A}$, same $I_{PG} = 1.5 \text{ kA}$ but opposite direction of the filter field current. Figures 7a and 7c present the plasma parameters obtained for the *standard* operation configuration, while the *reversed* configuration is presented in figures 7b and 7d. The standard configuration presents an increase of the densities of positive and negative ions from the bottom to the top. The positive ion density varies from $4.6 \times 10^{16} \text{ m}^{-3}$ to $9.2 \times 10^{16} \text{ m}^{-3}$, while the negative ion density ranges between $3.3 \times 10^{16} \text{ m}^{-3}$ to $6.5 \times 10^{16} \text{ m}^{-3}$, almost doubling its value from top to bottom. This agrees with the single beamlet current measurements reported in [18]: for this source condition the accelerated negative ion current also shows a similar top-bottom asymmetry. The cavity ring-down spectroscopy [16] estimation of the negative ion density was also available for this configuration, and its measurement is also reported in figure 7b (the green

point). Its value seems in agreement with the negative ion density trend seen by the probes. The potential difference between the sheath edge and the plasma grid is larger in correspondence of the top probe (2.9 V) with respect to the bottom measurement (0.8 V), while it is comparable for the two central segments. The electron temperature varies in the opposite direction, decreasing moving from the bottom segment (2.6 eV) to the top one (1.2 eV). The electron density instead has a minimum in correspondence of the second segment from the top (at 200 mm), and correspondingly the electronegativity reaches a value of 10.5.

In the reversed configuration all the trends are the opposite: the positive ion density in the bottom segment ($11.2 \times 10^{16} \text{ m}^{-3}$) is larger than that in the top segment ($3.4 \times 10^{16} \text{ m}^{-3}$). Negative ion density has a similar trend, but with a smaller excursion (from $6.5 \times 10^{16} \text{ m}^{-3}$ to $2.8 \times 10^{16} \text{ m}^{-3}$), and also the electron temperature decreases monotonically from the bottom to the top in this configuration (from $4.7 \times 10^{16} \text{ m}^{-3}$ to $0.5 \times 10^{16} \text{ m}^{-3}$). For this reason, the electronegativity does not show the same large variation as for the standard configuration, ranging from 1.8 at the bottom to 4.9 at the top. The trend of the electron temperature and sheath potential is also reversed, with a lower temperature (1.2 eV) and larger potential difference (1.7 V) at the bottom than at the top (2.0 eV and 0.3 eV).

4 Conclusion

Investigating negative ion production in a large negative ion source for fusion is a key aspect for improving source operation. In particular, negative ion density is usually measured using lasers with Cavity Ring-down spectroscopy or from optical measurements, with the drawback of obtaining only measurements integrated along one line of sight.

In this paper a fitting procedure for determining the negative ion density from Langmuir probe characteristics was presented, providing a localized measurement of negative ion density. We highlighted the importance of a correct determination of the different collection areas for the various plasma species, especially for the electrons, and applied the model to data collected during SPIDER campaigns. Using the measurement of a vertical array of Langmuir probes, it also allowed to estimate the vertical uniformity of plasma parameters across the plasma grid surface, confirming its dependence on the direction of the filter field current, in agreement with what was found by other diagnostics. The model also showed an agreement between the co-extracted electron current measurement and the electron density measurement of the probe in correspondence of the segment where the plasma density was larger during beam extraction phase. This can be an indication of the use of this analysis technique to assess the uniformity also of the heat load generated by the co-extracted electron current on the extraction grid.

In general, this approach for analyzing Langmuir probe data will provide a new tool to assess the spatial uniformity of negative ion production in a large negative ion source such as SPIDER, using the measurements performed with the bi-dimensional sets of Langmuir probe data embedded in the plasma grid and the bias plate.

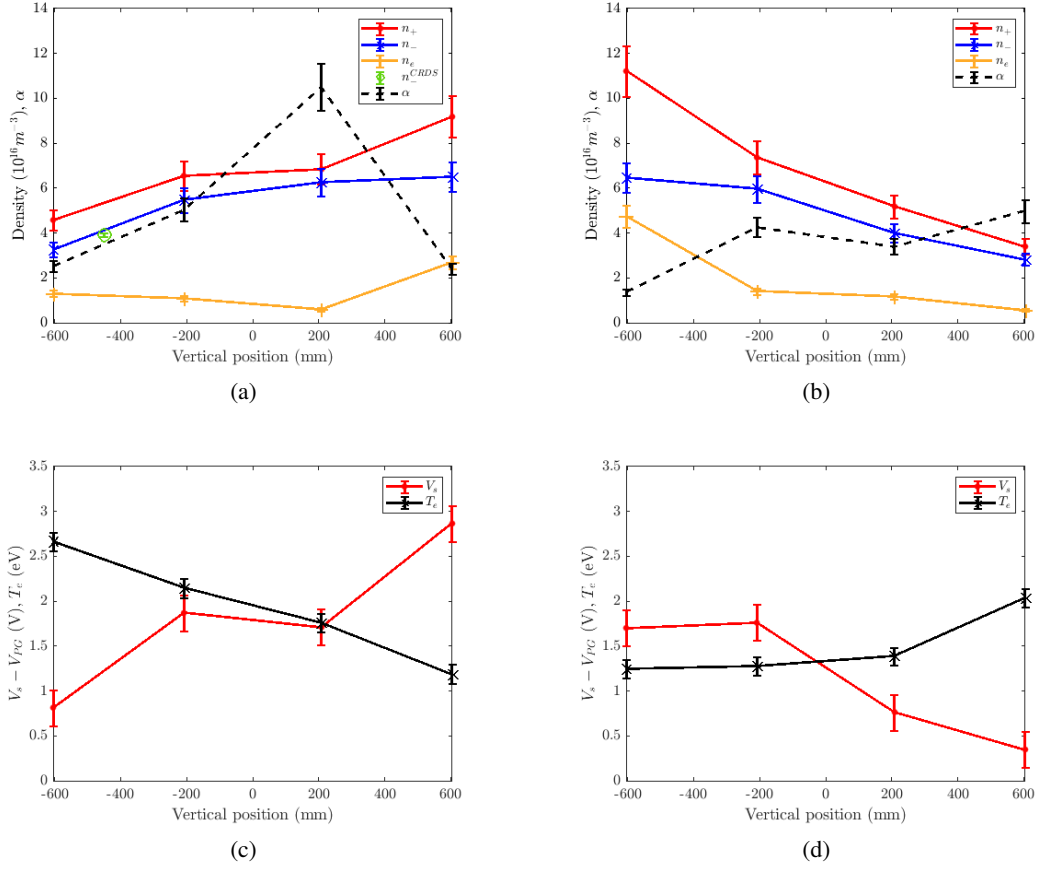


Figure 7: Vertical profile of plasma parameters measured for the *standard* (figure a for the densities and electronegativity and c for the electron temperature and sheath potential) and *reversed* (figure b for the densities and electronegativity and d for the electron temperature and sheath potential) configurations. The plasma pulse is performed with 50 kW/driver of RF power, $I_{BI} = 190$ A, $I_{BP} = 80$ A, 0.3 Pa of source filling pressure and 1.5 kA of filter field current, with opposite direction in the two configurations.

Acknowledgments

This work has been carried out within the framework of the ITER-RFX Neutral Beam Testing Facility (NBTF) Agreement and has received funding from the ITER Organization. The views and opinions expressed herein do not necessarily reflect those of the ITER Organization. This work has been carried out within the framework of the EUROfusion Consortium, funded by the European Union via the Euratom Research and Training Programme (Grant Agreement No 101052200 — EUROfusion). Views and opinions expressed are however those of the author(s) only and do not necessarily reflect those of the European Union or the European Commission. Neither the European Union nor the European Commission can be held responsible for them.

References

- [1] R. S. Hemsworth, D. Boilson, P. Blatchford, M. Dalla Palma, G. Chitarin, H. P. L. de Esch, F. Geli, M. Dremel, J. Graceffa, D. Marcuzzi, G. Serianni, D. Shah, M. Singh, M. Urbani and P. Zaccaria, *Overview of the design of the ITER heating neutral beam injectors*, *New J. Phys.* **19-2** (2017) 025005.
- [2] V. Toigo et al., *The ITER Neutral Beam Test Facility towards SPIDER operation*, *Nucl. Fusion* **57** (2017) 086027.
- [3] E. Sartori et al., *First operations with caesium of the negative ion source SPIDER*, *Nucl. fusion*, **62** (2022) 086022.
- [4] A. Zamengo, M. Bigi, A. Maistrello and M. Recchia, *Power supply system for large negative ion sources: Early operation experience on the SPIDER experiment*, *Fus. Eng. Des.* **173** (2021) 112790.
- [5] A. Rizzolo, M. Barbisan, L. Bizzotto, et al., *Characterization of the SPIDER Cs oven prototype in the CAesium Test stand for the ITER HNB negative ion sources*, *Fusion Eng. Des.*, **146** (2019), 676.
- [6] M. Fadone, B. Pouradier Duteil, E. Sartori, C. Gasparrini, C. Cavallini, V. Candela, A. Rizzolo and M. Barbisan, *Summary of caesium evaporation and deposition during SPIDER first campaign*, submitted to *JINST*, (2022).
- [7] M. Spolaore, G. Serianni, A. Leorato and F. Degli Agostini, *Design of a system of electrostatic probes for the RF negative ion source of the SPIDER experiment*, *J. Phys. D: Appl. Phys.* **43** (2010) 124018.
- [8] M. Brombin, M. Spolaore, G. Serianni, N. Pomaro, C. Taliercio, M. Dalla Palma, R. Pasqualotto and L. Schiesko, *Langmuir probes for SPIDER experiment: tests in BATMAN*, *Rev. Sci. Instrum.* **85** (2014) 02A715.
- [9] C. Poggi, M. Spolaore, M. Brombin, R. Cavazzana, M. Fadone, R. Pasqualotto, A. Pimazzoni, N. Pomaro, E. Sartori, G. Serianni and C. Taliercio, *Langmuir probes as a tool to investigate plasma uniformity in a large negative ion source*, *IEEE Trans. Pl. Sci.* **50-11** (2021) 3890-3896.
- [10] J. Bredin, P. Chabert and A. Aanesland, *Langmuir probe analysis in electronegative plasmas*, *Phys. of Plasmas* **21** (2014) 123502.
- [11] P. Chabert and N. Braithwaite, *Physics of Radio-Frequency Plasmas*, Cambridge Univ. Press (2011).
- [12] M.A. Lieberman and A.J. Lichtenberg, *Principles of Plasma Discharges and Materials Processing*, John Wiley & Sons, Inc. (2005).
- [13] N. Marconato, E. Sartori and G. Serianni, *Numerical and Experimental Assessment of the New Magnetic Field Configuration in SPIDER*, *IEEE Trans. Pl. Sci.* **50**, (2012-11) 3884-3889
- [14] M. Usoltceva, E. Faudot, S. Devaux, S. Heuraux, J. Ledig, G. V. Zadvitskiy, R. Ochoukov, K. Crombé and J.-M. Noterdaeme, *Effective collecting area of a cylindrical Langmuir probe in magnetized plasma*, *Phys. of Plasmas* **25** (2018) 063518.
- [15] L. Schiesko, P. McNeely, P. Franzen and U. Fantz, *Magnetic field dependence of the plasma properties in a negative hydrogen ion source for fusion*, *Plasma Phys. Control. Fusion* **54**, (2012-10) 105002
- [16] M. Barbisan, R. Pasqualotto, R. Agnello, M. Pilioci, G. Serianni, C. Taliercio, V. Cervaro, F. Rossetto and A. Tiso, *Development and first operation of a cavity ring down spectroscopy diagnostic in the negative ion source SPIDER*, *Rev. Sci. Instrum.* **92**, (2021-05) 053507
- [17] G. Serianni et. al., *Spatially resolved diagnostics for optimization of large ion beam sources*, *Rev. Sci. Instrum* **93**, (2022-08) 081101

- [18] A. Shepherd et. al., *Beam homogeneity of caesium seeded SPIDER using direct beamlet current measurement, accepted for publication on Fusion Engineering and Design*